Journal of Renewable Materials

Tech Science Press

DOI: 10.32604/jrm.2021.015166

ARTICLE

Characterization of the Flexural Behavior of Bamboo Beams

Limin Tian[1,2], Jianpeng Wei[3], Jiping Hao[1,*] and Qiushuo Wang[1]

[1]School of Civil Engineering, Shaanxi Key Laboratory of Structure and Earthquake Resistance, Xi'an University of Architecture and Technology, Xi'an, 710055, China

[2]The Key Laboratory of Plateau Building and Eco-Community in Qinghai, Qinghai Building and Materials Research Co., Ltd., Xining, 810008, China

[3]Anhui Province Key Laboratory of Green Building and Assembly Construction, Anhui Institute of Building Research & Design, Hefei, 230031, China

[*]Corresponding Author: Jiping Hao. Email: haojiping@xauat.edu.cn

Received: 27 November 2020 Accepted: 19 February 2021

ABSTRACT

Bamboo is a renewable and environmentally friendly material often used for construction. This study investigates the flexural behavior of bamboo beams through theoretical and finite element (FE) analyses. Considering the material's nonlinearity, a method of calculating load-deflection curves is proposed and validated via FE analysis. The interfacial slippage dominated by the shear stiffness of the interface between two bamboo poles significantly influences the flexural behavior of double-pole bamboo beams. Thus, the load-deflection curves for different shear stiffnesses can be obtained via theoretical and FE analyses. Subsequently, a novel configuration using diagonal steel bands to avoid slippage is presented. An inclination angle of 45° is suggested to adequately develop the stiffness and bearing capacity of the steel band.

KEYWORDS

Bamboo beam; flexural behavior; interfacial slippage; steel band; FE analysis

1 Introduction

Bamboo is a sustainable material used in the construction of buildings [1,2]. It is renewable and environmentally friendly. Its growth speed and strength are greater than those of timber. Bamboo is a typical anisotropic material. García et al. [3] and Akinbade et al. [4] studied the transverse properties of bamboo, testing the elastic constants and tensile capacity in the transverse direction. The longitudinal properties of bamboo were also investigated. Liu et al. [5] measured the longitudinal tensile strength and elastic modulus. Qiu et al. [6] constructed a longitudinal constitutive model using the Ramberg–Osgood relation. These studies indicated that the tensile strength of bamboo in the longitudinal direction was close to the strength of steel while the elastic modulus of bamboo was approximately one-twentieth of that of steel. Hence, bamboo is considered suitable for use as a centrally stressed member [7–12]. As one of the most important members of a structure, understanding the flexural behavior of bamboo beams is extremely important to increase their application in construction [2,13]. Currently, two types of bamboo beams have been widely studied: Original and engineered bamboo beams.

For original bamboo beams, the natural shape of the bamboo is maintained; this advantage can be exploited in structures. García-Aladín et al. [14,15] conducted bending tests on single and double bamboo poles to calculate their shear moduli and stiffnesses. Trujillo et al. [16] implemented more than 200 bending tests on bamboo poles, which were used for bamboo strength grading. Nurmadina et al. [17] adopted three-point bending tests to obtain the bending stiffness of a single bamboo pole. Lorenzo et al. [18] proposed an analytical bimodulus model to determine the strain and stress distribution of a single bamboo beam. These studies indicated that owing to the deflection limit, it was difficult to achieve large spans using a single bamboo pole as a beam [19,20]. Considering the superiority of original bamboo, a bionic bamboo beam, including tubes and diaphragms, was invented [21,22]. Its bending model was deduced using Euler-Bernoulli beam theory.

To increase the applicability of original bamboo beams, Tian et al. [23] presented a composite mortar-sprayed bamboo beam. The results demonstrated that interfacial slippage between two bamboo poles was difficult to avoid and the composite effect could not be fully exploited. Therefore, bolted connections are commonly applied to avoid interfacial slip [24–28]. Conversely, the engineered bamboo beam is a new bamboo product, the section of which can be varied and the bending stiffness can be determined according to the design requirement [29,30]. Huang et al. [31] and Li et al. [32] analyzed the flexural behavior of engineered bamboo beams and their ultimate bearing capacity and deformation were deduced. Furthermore, engineered bamboo can be effectively combined with other materials (i.e., steel, concrete, and timber) to form new composite bamboo beams. Wei et al. [33] and Wang et al. [34] proposed a fiber-reinforced engineered bamboo beam and a bamboo-concrete composite beam, respectively. Zhong et al. [35] and Wei et al. [36] adopted steel bars to enhance the engineered bamboo beam. Li et al. [37] presented an I-section bamboo-steel composite beam. However, producing engineered bamboo is energy consuming and the process is not environmentally friendly.

To completely exploit the excellent performance of original bamboo beams, this study investigated the flexural behavior of single-pole and double-pole bamboo beams via theoretical analysis. Simultaneously, the influence of interfacial slippage was analyzed. Then, an effective configuration to avoid slippage without destroying the original bamboo was proposed and validated.

2 Flexural Behavior Analysis

2.1 Constitutive Model Along the Grain

The flexural behavior of bamboo beams is directly related to the constitutive model of bamboo along the grain, as shown in Fig. 1 and Eq. (1). E_t and E_c represent the elastic moduli in the tensile and compressive states, respectively; σ_{tu} and σ_{cu} denote the ultimate stresses; ε_{tu} and ε_{cu} define the ultimate strains. ε_{cp} denotes the strain at the compressive yield point. The constitutive model includes two aspects: Tension and compression [6,31,32]. Based on previous tests [3–6], bamboo exhibits a linear elastic strain-stress relationship in the tensile state and fractures occur corresponding to the ultimate stress. There is almost no plastic deformation stage. Bamboo approximates an ideal elastoplastic material under a compressive load. Moreover, the elastic modulus in the tensile state is always greater than that under compression.

$$\sigma(\varepsilon) = \begin{cases} -\sigma_{cu} & -\varepsilon_{cu} \le \varepsilon \le -\varepsilon_{cp} \\ E_c\varepsilon & -\varepsilon_{cp} \le \varepsilon \le 0 \\ E_t\varepsilon & 0 \le \varepsilon \le \varepsilon_{tu} \end{cases} \tag{1}$$

2.2 Curvature of a Single-Pole Bamboo Beam

2.2.1 Elastic Stage

Fig. 2 presents the stress and strain distributions in the elastic stage for a single-pole bamboo beam, conforming to the plane-section assumption. Owing to the greater elastic modulus in the tensile zone, the

neutral axis is below the midline of the beam. The cross-section of bamboo is assumed to be an ideal annulus with invariable thickness. A polar coordinate system is established such that the origin of the coordinate system is located at the center of the section and the lower part of the vertical symmetry axis is used as the polar axis.

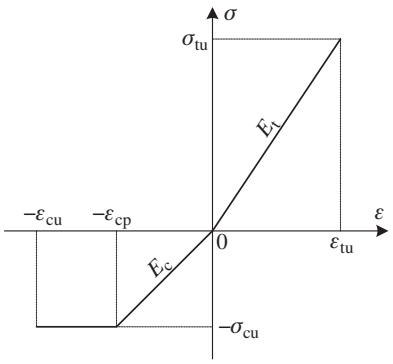

Figure 1: The constitutive model of bamboo along the grain

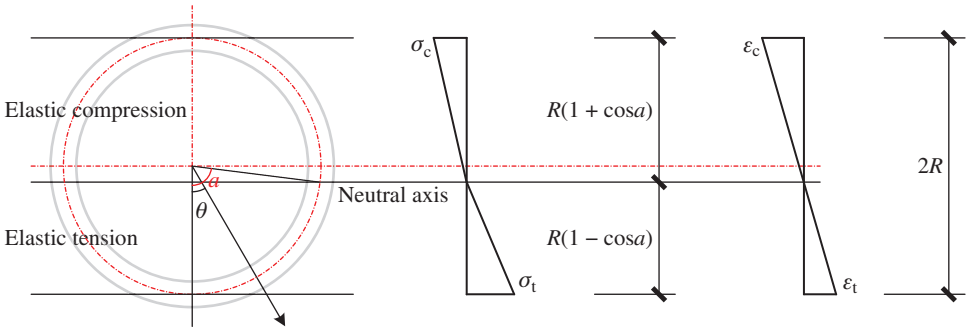

Figure 2: Stress and strain distributions during the elastic stage

The strain and stress on the central line of the annulus are adopted to represent the strain and stress at the same polar angle. Thus, the area integral can be simplified as the arc integral in the following deduction. Eq. (2) expresses the stress distribution along the central line of the annulus, where the stress is a function of the polar angle.

$$\sigma(\theta) = \begin{cases} \dfrac{\cos\theta - \cos a}{1 - \cos a}\sigma_t & 0 \le \theta \le a \\ \dfrac{\cos\theta - \cos a}{\beta(1 - \cos a)}\sigma_t & a \le \theta \le \pi \end{cases} \quad (\beta = E_t/E_c \quad \beta \ge 1) \tag{2}$$

where σ_t is the tensile stress at the bottom surface and θ is the polar angle. The polar angle a corresponds to the location of the neutral axis. β is the ratio of E_t to E_c. The polar angle a can be calculated by the longitudinal force equilibrium, as follows:

$$\int_0^{\pi} \sigma(\theta) R t \mathrm{d}\theta = 0 \tag{3}$$

$$\int_0^a \frac{\cos\theta-\cos a}{1-\cos a}\sigma_t R t\mathrm{d}\theta+\int_a^\pi \frac{\cos\theta-\cos a}{\beta(1-\cos a)}\sigma_t R t\mathrm{d}\theta=0 \tag{4}$$

$$\frac{\sin a-a\cos a}{1-\cos a}+\frac{-\pi\cos a-\sin a+a\cos a}{\beta(1-\cos a)}=0 \tag{5}$$

$$\tan a-a=\frac{\pi}{\beta-1} \tag{6}$$

where R is the radius of the central line of the annulus and t is the thickness of the annulus. In Eq. (6), the polar angle a is only relevant to β, illustrating that the neutral axis does not change during the elastic stage. The bending moment in this section is expressed as follows:

$$\int_0^\pi \sigma(\theta)(\cos\theta-\cos a)R^2 t\mathrm{d}\theta=M/2 \tag{7}$$

$$\int_0^a \frac{(\cos\theta-\cos a)^2}{1-\cos a}\sigma_t R^2 t\mathrm{d}\theta+\int_a^\pi \frac{(\cos\theta-\cos a)^2}{\beta(1-\cos a)}\sigma_t R^2 t\mathrm{d}\theta=M/2 \tag{8}$$

$$\frac{-0.75\sin 2a+0.5a+a\cos^2 a}{1-\cos a}+\frac{0.5\pi+\pi\cos^2 a+0.75\sin 2a-0.5a-a\cos^2 a}{\beta(1-\cos a)}=\frac{M}{2\sigma_t R^2 t} \tag{9}$$

$$\lambda=\frac{-0.75\sin 2a+0.5a+a\cos^2 a}{1-\cos a}+\frac{0.5\pi+\pi\cos^2 a+0.75\sin 2a-0.5a-a\cos^2 a}{\beta(1-\cos a)} \tag{10}$$

$$M=2\lambda\sigma_t R^2 t \tag{11}$$

When the polar angle a is solved using Eq. (6), the constant coefficient λ can be obtained using Eq. (10). Then, the bending moment can be obtained using Eq. (11). The bending moment is proportional to σ_t. The relationship between strain and the neutral axis displayed in Fig. 2 leads to:

$$\frac{\varepsilon_t}{\varepsilon_c}=\frac{\sigma_t E_c}{\sigma_c E_t}=\frac{\alpha_e}{\beta}=\frac{1-\cos a}{1+\cos a}\left(\alpha_e=\sigma_t/\sigma_c \quad \sigma_c\le\sigma_{cu}\right) \tag{12}$$

where ε_t represents the tensile strain at the bottom surface and ε_c signifies the compressive strain at the top surface. Substituting $\sigma_t=\alpha_e\sigma_{cu}$ into Eq. (11) yields:

$$M_p=2\lambda\alpha_e\sigma_{cu}R^2 t=2\lambda\beta\frac{1-\cos a}{1+\cos a}\sigma_{cu}R^2 t \tag{13}$$

where M_p is the maximum bending moment of the elastic stage. When the bending moment is smaller than M_p, the curvature can be calculated as follows:

$$k_e=\frac{\sigma_t}{E_t(1-\cos a)R}=\frac{M}{2\lambda(1-\cos a)E_t R^3 t} \quad M\le M_p \tag{14}$$

2.2.2 Elastic-Plastic Stage

Fig. 3 shows the stress and strain distributions during the elastic-plastic stage. The cross-section of bamboo comprises three areas: Elastic tension, elastic compression, and plastic compression. Two dividing lines, corresponding to angles a and b, divide the three areas.

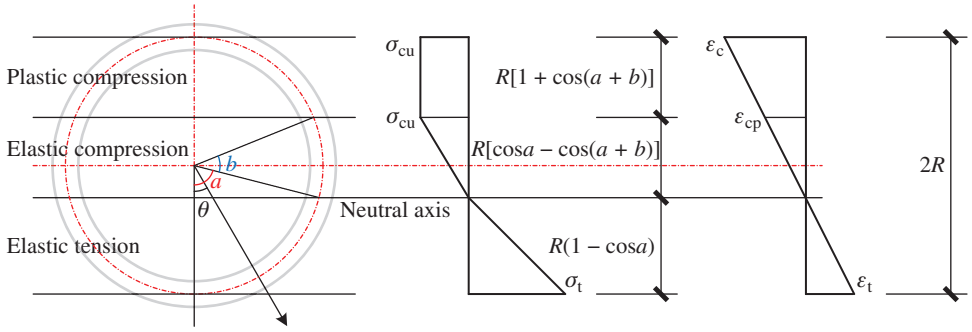

Figure 3: Stress and strain distributions during the elastic-plastic stage

Eq. (15) expresses the stress distribution during the elastic-plastic stage, which comprises three parts.

$$\sigma(\theta)=\begin{cases}\dfrac{\cos\theta-\cos a}{1-\cos a}\sigma_{\mathrm{t}} & 0\le\theta\le a\\ \dfrac{\cos\theta-\cos a}{\beta(1-\cos a)}\sigma_{\mathrm{t}} & a\le\theta\le a+b\\ -\sigma_{\mathrm{cu}} & (a+b)\le\theta\le\pi\end{cases}\tag{15}$$

Considering the deformation relationship over the section yields:

$$\frac{\varepsilon_{\mathrm{t}}}{\varepsilon_{\mathrm{cp}}}=\frac{\sigma_{\mathrm{t}}E_{\mathrm{c}}}{\sigma_{\mathrm{cu}}E_{\mathrm{t}}}=\frac{\alpha_{\mathrm{p}}}{\beta}=\frac{1-\cos a}{\cos a-\cos(a+b)}\left(\alpha_{\mathrm{p}}=\sigma_{\mathrm{t}}/\sigma_{\mathrm{cu}}\quad\alpha_{\mathrm{e}}\sigma_{\mathrm{cu}}\le\sigma_{\mathrm{t}}\le\sigma_{\mathrm{tm}}\right)\tag{16}$$

$$b=\arccos[\cos a-\frac{\beta}{\alpha_{\mathrm{p}}}(1-\cos a)]-a\tag{17}$$

where σ_{tm} is the maximum value of σ_{t}. The force equilibrium along the longitudinal direction yields.

$$\int_0^{\pi}\sigma(\theta)Rt\mathrm{d}\theta=0\tag{18}$$

$$\int_0^{a}\frac{\cos\theta-\cos a}{1-\cos a}\sigma_{\mathrm{t}}Rt\mathrm{d}\theta+\int_a^{a+b}\frac{\cos\theta-\cos a}{\beta(1-\cos a)}\sigma_{\mathrm{t}}Rt\mathrm{d}\theta+\int_{a+b}^{\pi}-\sigma_{\mathrm{cu}}Rt\mathrm{d}\theta=0\tag{19}$$

$$\frac{\sin a-a\cos a}{1-\cos a}+\frac{\sin(a+b)-\sin a-b\cos a}{\beta(1-\cos a)}-\frac{\pi-a-b}{\alpha_{\mathrm{p}}}=0\tag{20}$$

The bending moment of the section is expressed as

$$\int_0^{\pi}\sigma(\theta)(\cos\theta-\cos a)R^2t\mathrm{d}\theta=M/2\tag{21}$$

$$\int_0^{a}\frac{(\cos\theta-\cos a)^2}{1-\cos a}\sigma_{\mathrm{t}}R^2t\mathrm{d}\theta+\int_a^{a+b}\frac{(\cos\theta-\cos a)^2}{\beta(1-\cos a)}\sigma_{\mathrm{t}}R^2t\mathrm{d}\theta+\int_{a+b}^{\pi}-\sigma_{\mathrm{cu}}(\cos\theta-\cos a)R^2t\mathrm{d}\theta=M/2\tag{22}$$

$$\frac{-0.75\sin 2a + 0.5a + a\cos^2 a}{1-\cos a} + \frac{0.25\sin 2(a+b) - 2\sin(a+b)\cos a + 0.75\sin 2a + 0.5b + b\cos^2 a}{\beta(1-\cos a)} + \frac{\pi\cos a + \sin(a+b) - (a+b)\cos a}{\alpha_p} = \frac{M}{2\sigma_t R^2 t} \tag{23}$$

$$\gamma = \frac{-0.75\sin 2a + 0.5a + a\cos^2 a}{1-\cos a} + \frac{0.25\sin 2(a+b) - 2\sin(a+b)\cos a + 0.75\sin 2a + 0.5b + b\cos^2 a}{\beta(1-\cos a)} + \frac{\pi\cos a + \sin(a+b) - (a+b)\cos a}{\alpha_p} \tag{24}$$

$$M = 2\gamma\sigma_t R^2 t \tag{25}$$

where the constant coefficient γ in Eq. (24) is related to a, b, and α_p. When the bending moment M is given, the unknown variables a, b, and α_p can be solved using Eqs. (17), (20), and (23). Two types of failures are considered in the ultimate state: Tensile and compressive failures. If the compressive failure occurs at the top surface of the section, $\varepsilon_t = \frac{1-\cos a}{1+\cos a}\varepsilon_{cu}$ will not exceed ε_{tu}. Substituting $\alpha_p = \sigma_{tm}/\sigma_{cu} = E_t \min(\frac{1-\cos a}{1+\cos a}\varepsilon_{cu}, \varepsilon_{tu})/\sigma_{cu}$ into Eqs. (17), (20), and (23) yields:

$$M_u = 2\gamma\sigma_{tm} R^2 t = \min(\frac{1-\cos a}{1+\cos a}\varepsilon_{cu}, \varepsilon_{tu}) 2\gamma E_t R^2 t \tag{26}$$

where M_u is the ultimate bending moment. When the bending moment is greater than M_p and smaller than M_u, the curvature can be calculated as follows:

$$k_p = \frac{\sigma_t}{E_t(1-\cos a)R} = \frac{M}{2\gamma(1-\cos a)E_t R^3 t} \quad M_p \le M \le M_u \tag{27}$$

2.3 Curvature of a Double-Pole Bamboo Beam

There are also two curvature stages for a double-pole bamboo beam. Owing to the cross-section containing two annuli, the elastic stage can be considered for two cases and the elastic-plastic stage for four. Two polar coordinate systems are separately established for the top and bottom bamboo poles. *a* and *b* determine the location of the neutral axis and the boundary of the elastic and plastic areas, as displayed below in six different diagrams (Figs. 4–9) illustrating the stress and strain distributions. The curvature analysis of a single-pole bamboo beam can be referenced for a double-pole bamboo beam. Therefore, the description of the curvature analysis process is not repeated but the main equations and results are presented as follows.

2.3.1 Elastic Stage

The location of the neutral axis differentiates the two cases. The neutral axis is located between the centerlines of the two annuli in Case 1; the neutral axis in Case 2 intersects the centerline of the bottom bamboo pole.

(1) Case 1:

Fig. 4 shows the stress and strain distributions in Case 1.

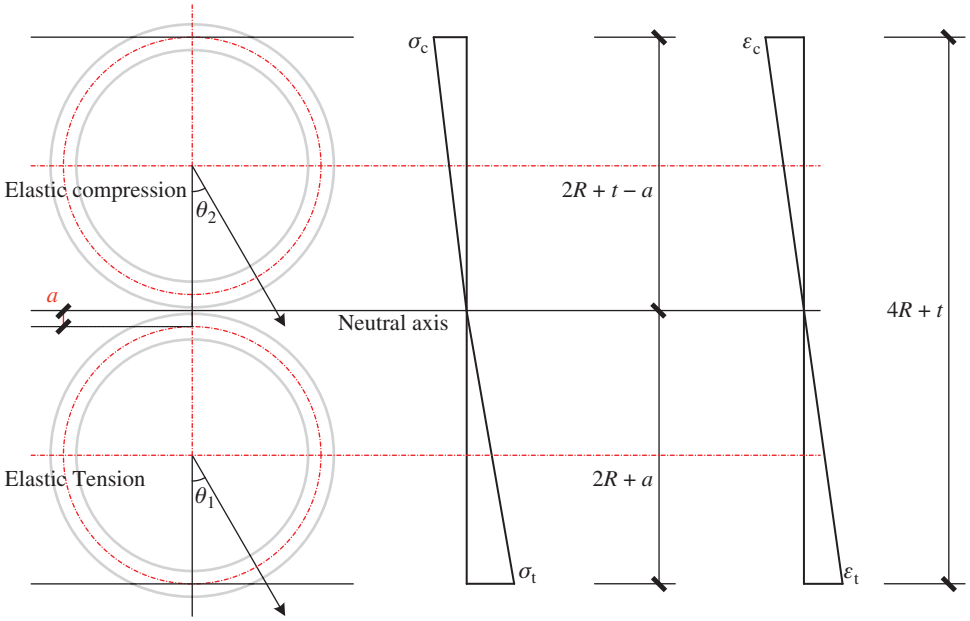

Figure 4: Stress and strain distributions in Case 1

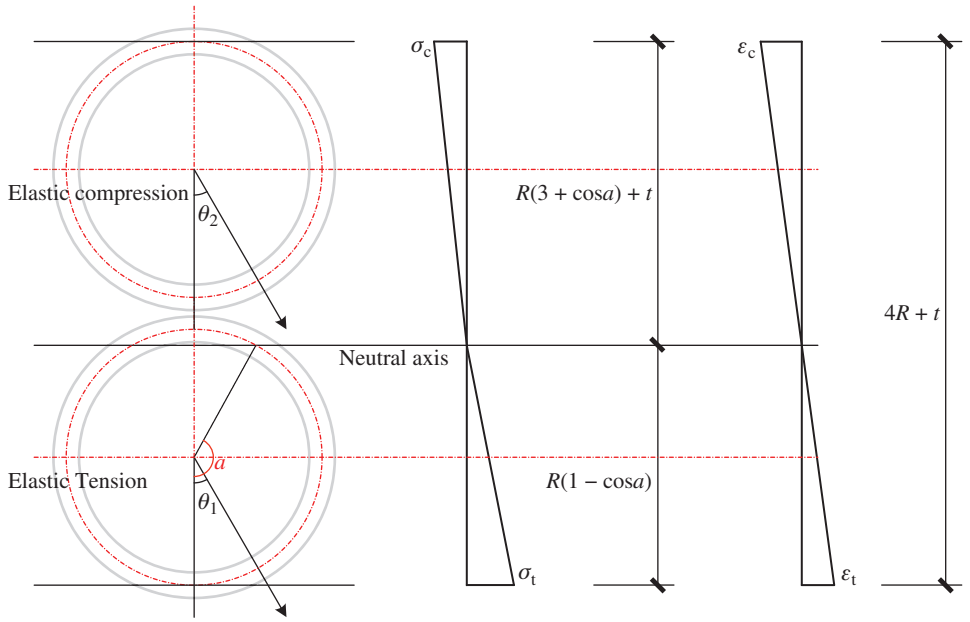

Figure 5: Stress and strain distributions in Case 2

Eqs. (28)–(32) express the curvature analysis of a double-pole bamboo beam in Case 1.

$$a = \frac{R(1-\beta)+t}{1+\beta} \quad 0 \le a \le 0.5t \tag{28}$$

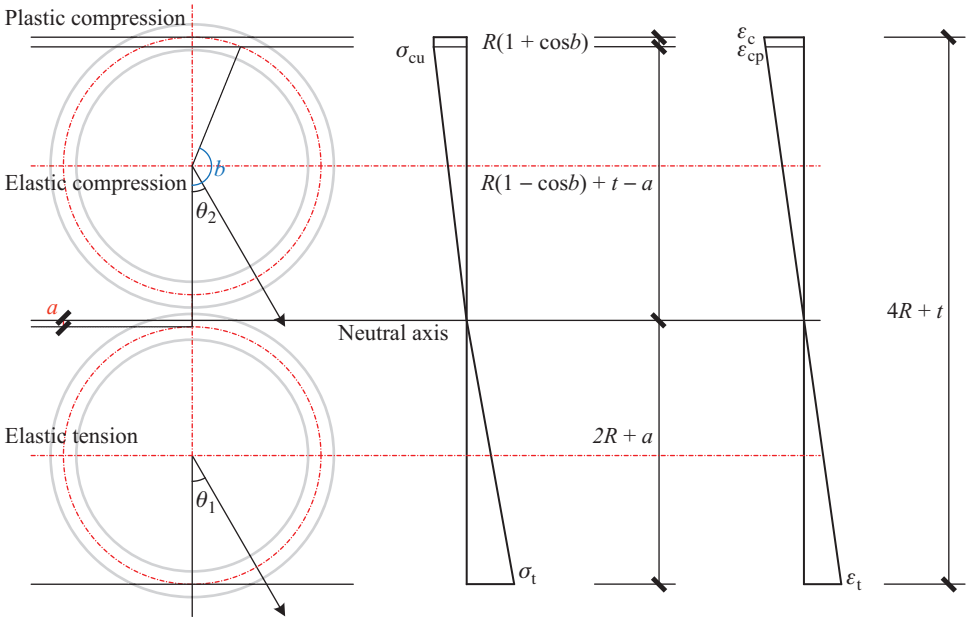

Figure 6: Stress and strain distributions in Case 3

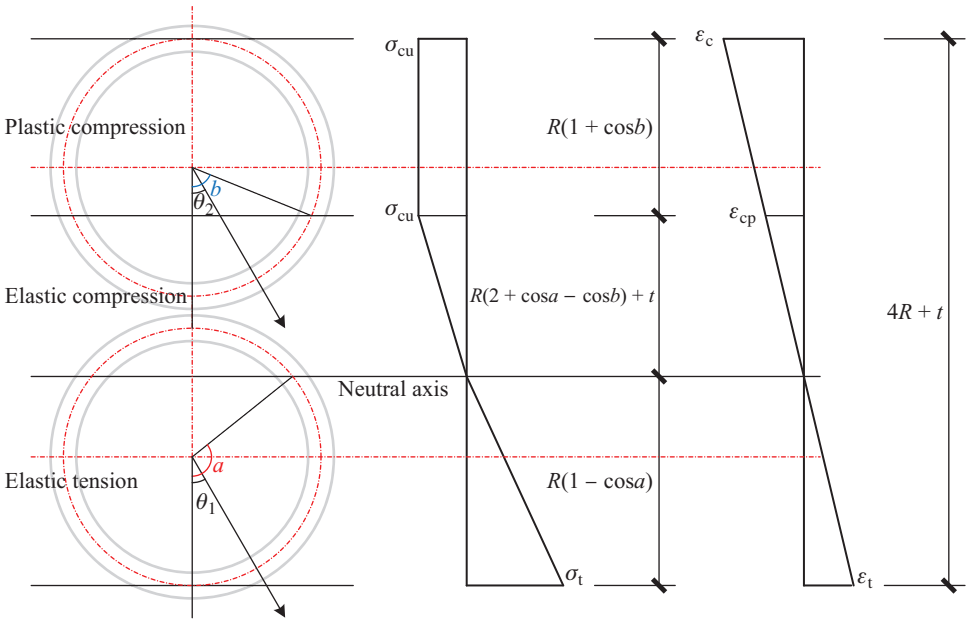

Figure 7: Stress and strain distributions in Case 4

$$\lambda = \frac{0.5\pi R^2 + \pi(R+a)^2}{2R^2 + aR} + \frac{0.5\pi R^2 + \pi(R+t-a)^2}{\beta(2R^2+aR)} \tag{29}$$

$$\frac{\varepsilon_t}{\varepsilon_c} = \frac{\sigma_t E_c}{\sigma_c E_t} = \frac{\alpha_e}{\beta} = \frac{2R+a}{2R+t-a} \tag{30}$$

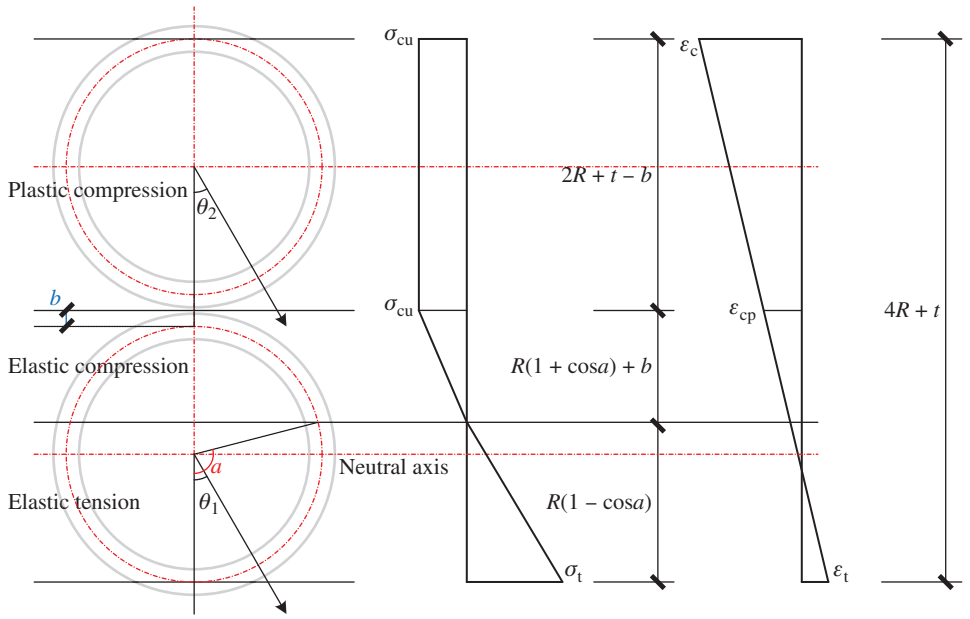

Figure 8: Stress and strain distributions in Case 5

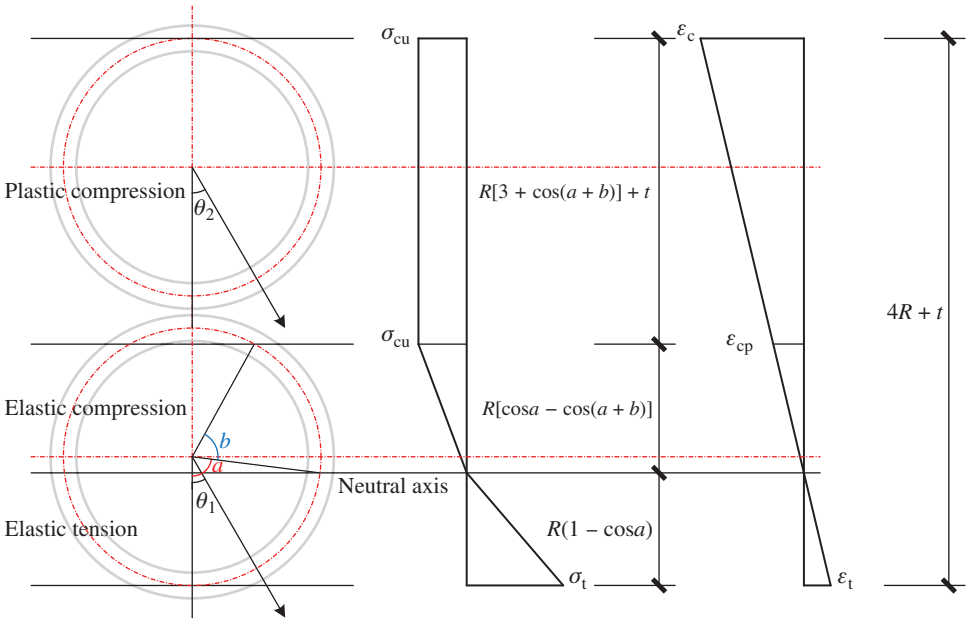

Figure 9: Stress and strain distributions in Case 6

$$M_p = 2\lambda\alpha_e\sigma_{cu}R^2t = 2\lambda\beta\frac{2R+a}{2R+t-a}\sigma_{cu}R^2t \tag{31}$$

$$k_e = \frac{\sigma_t}{E_t(2R+a)} = \frac{M}{2\lambda(2R+a)E_tR^2t} \quad M \le M_p \tag{32}$$

(2) Case 2

Fig. 5 shows the stress and strain distributions in Case 2.

Eqs. (33)–(37) express the curvature analysis of a double-pole bamboo beam in Case 2.

$$\frac{2\pi R(1+\cos a)+\pi t}{R(\sin a - a\cos a)} = \beta - 1 \tag{33}$$

$$\lambda = \frac{-0.75\sin 2a + 0.5a + a\cos^2 a}{1-\cos a} + \frac{0.5\pi + \pi\cos^2 a + 0.75\sin 2a - 0.5a - a\cos^2 a}{\beta(1-\cos a)} + \frac{0.5\pi R^2 + \pi(R\cos a + 2R + t)^2}{\beta R^2(1-\cos a)} \tag{34}$$

$$\frac{\varepsilon_t}{\varepsilon_c} = \frac{\sigma_t E_c}{\sigma_c E_t} = \frac{\alpha_e}{\beta} = \frac{R(1-\cos a)}{R(3+\cos a)+t} \tag{35}$$

$$M_p = 2\lambda\alpha_e\sigma_{cu}R^2 t = 2\lambda\beta\frac{R(1-\cos a)}{R(3+\cos a)+t}\sigma_{cu}R^2 t \tag{36}$$

$$k_e = \frac{\sigma_t}{E_t(1-\cos a)R} = \frac{M}{2\lambda(1-\cos a)E_t R^3 t} \quad M \le M_p \tag{37}$$

2.3.2 Elastic-Plastic Stage

The neutral axis and boundary of the elastic and plastic areas differentiate the four cases.

(1) Case 3

Fig. 6 shows the stress and strain distributions in Case 3.

Eqs. (38)–(43) express the curvature analysis of a double-pole bamboo beam in Case 3.

$$\frac{\varepsilon_t}{\varepsilon_{cp}} = \frac{\sigma_t E_c}{\sigma_{cu}E_t} = \frac{\alpha_p}{\beta} = \frac{2R+a}{R(1-\cos b)+t-a} \tag{38}$$

$$b = \arccos[1 + \frac{t-a}{R} - \frac{\beta}{\alpha_p}(2+\frac{a}{R})] \tag{39}$$

$$\frac{\pi(R+a)}{2R+a} + \frac{R\sin b - b(R+t-a)}{\beta(2R+a)} - \frac{\pi - b}{\alpha_p} = 0 \tag{40}$$

$$\gamma = \frac{0.5\pi R^2 + \pi(R+a)^2}{2R^2+aR} + \frac{0.25R^2\sin 2b + 0.5bR^2 - 2(R+t-a)R\sin b + b(R+t-a)^2}{\beta(2R^2+aR)} + \frac{(R+t-a)(\pi - b) + R\sin b}{R\alpha_p} \tag{41}$$

$$M_u = 2\gamma\sigma_{tm}R^2 t = \min(\frac{2R+t-a}{2R+a}\varepsilon_{cu}, \varepsilon_{tu})2\gamma E_t R^2 t \tag{42}$$

$$k_p = \frac{\sigma_t}{E_t(2R+a)} = \frac{M}{2\gamma(2R+a)E_t R^2 t} \tag{43}$$

(2) Case 4

Fig. 7 displays the stress and strain distributions in Case 4.

Eqs. (44)–(49) express the curvature analysis of a double-pole bamboo beam in Case 4.

$$\frac{\varepsilon_t}{\varepsilon_{cp}}=\frac{\sigma_t E_c}{\sigma_{cu}E_t}=\frac{\alpha_p}{\beta}=\frac{R(1-\cos a)}{R(2+\cos a-\cos b)+t} \tag{44}$$

$$b=\arccos[2+\cos a+\frac{t}{R}-\frac{\beta}{\alpha_p}(1-\cos a)] \tag{45}$$

$$\frac{\sin a-a\cos a}{1-\cos a}+\frac{-\pi\cos a-\sin a+a\cos a}{\beta(1-\cos a)}+\frac{R\sin b-b(R\cos a+2R+t)}{\beta R(1-\cos a)}-\frac{\pi-b}{\alpha_p}=0 \tag{46}$$

$$\begin{aligned}\gamma=&\frac{-0.75\sin 2a+0.5a+a\cos^2 a}{1-\cos a}+\frac{0.5\pi+\pi\cos^2 a+0.75\sin 2a-0.5a-a\cos^2 a}{\beta(1-\cos a)}\\&+\frac{R^2(0.25\sin 2b+0.5b)-2R(R\cos a+2R+t)\sin b+b(R\cos a+2R+t)^2}{\beta R^2(1-\cos a)}\\&+\frac{(R\cos a+2R+t)(\pi-b)+R\sin b}{R\alpha_p}\end{aligned} \tag{47}$$

$$M_u=2\gamma\sigma_{tm}R^2t=\min(\frac{R(1-\cos a)}{R(3+\cos a)+t}\varepsilon_{cu},\varepsilon_{tu})2\gamma E_tR^2t \tag{48}$$

$$k_p=\frac{\sigma_t}{E_t(1-\cos a)R}=\frac{M}{2\gamma(1-\cos a)E_tR^3t} \tag{49}$$

(3) Case 5

Fig. 8 illustrates the stress and strain distributions in Case 5.

Eqs. (50)–(55) express the curvature analysis of a double-pole bamboo beam in Case 5.

$$\frac{\varepsilon_t}{\varepsilon_{cp}}=\frac{\sigma_t E_c}{\sigma_{cu}E_t}=\frac{\alpha_p}{\beta}=\frac{R(1-\cos a)}{R(1+\cos a)+b} \tag{50}$$

$$b=\frac{\beta}{\alpha_p}R(1-\cos a)-R(1+\cos a) \tag{51}$$

$$\frac{\sin a-a\cos a}{1-\cos a}+\frac{-\pi\cos a-\sin a+a\cos a}{\beta(1-\cos a)}-\frac{\pi}{\alpha_p}=0 \tag{52}$$

$$\gamma=\frac{-0.75\sin 2a+0.5a+a\cos^2 a}{1-\cos a}+\frac{0.5\pi+\pi\cos^2 a+0.75\sin 2a-0.5a-a\cos^2 a}{\beta(1-\cos a)}+\frac{\pi(R\cos a+2R+t)}{R\alpha_p} \tag{53}$$

$$M_u=2\gamma\sigma_{tm}R^2t=\min(\frac{R(1-\cos a)}{R(3+\cos a)+t}\varepsilon_{cu},\varepsilon_{tu})2\gamma E_tR^2t \tag{54}$$

$$k_p=\frac{\sigma_t}{E_t(1-\cos a)R}=\frac{M}{2\gamma(1-\cos a)E_tR^3t} \tag{55}$$

(4) Case 6

Fig. 9 shows the stress and strain distributions in Case 6.

Eqs. (56)–(61) express the curvature analysis of a double-pole bamboo beam in Case 6.

$$\frac{\varepsilon_t}{\varepsilon_{cp}} = \frac{\sigma_t E_c}{\sigma_{cu} E_t} = \frac{\alpha_p}{\beta} = \frac{1-\cos a}{\cos a - \cos(a+b)} \tag{56}$$

$$b = \arccos[\cos a - \frac{\beta}{\alpha_p}(1-\cos a)] - a \tag{57}$$

$$\frac{\sin a - a\cos a}{1-\cos a} + \frac{\sin(a+b) - \sin a - b\cos a}{\beta(1-\cos a)} - \frac{2\pi - a - b}{\alpha_p} = 0 \tag{58}$$

$$\gamma = \frac{-0.75\sin 2a + 0.5a + a\cos^2 a}{1-\cos a} + \frac{0.25\sin 2(a+b) - 2\sin(a+b)\cos a + 0.75\sin 2a + 0.5b + b\cos^2 a}{\beta(1-\cos a)} + \frac{\pi\cos a + \sin(a+b) - (a+b)\cos a}{\alpha_p} + \frac{\pi(R\cos a + 2R + t)}{R\alpha_p} \tag{59}$$

$$M_u = 2\gamma\sigma_{tm}R^2 t = \min(\frac{R(1-\cos a)}{R(3+\cos a)+t}\varepsilon_{cu}, \varepsilon_{tu})2\gamma E_t R^2 t \tag{60}$$

$$k_p = \frac{\sigma_t}{E_t(1-\cos a)R} = \frac{M}{2\gamma(1-\cos a)E_t R^3 t} \tag{61}$$

2.4 Load-Deflection Curves

For a simply supported beam, the bending moment is easily plotted. Fig. 10a shows the bending moment diagram under an external load $M(P,x)$ and Fig. 10b shows the bending moment diagram under the unit load $\overline{M}(x)$. According to the relationship between the curvature and bending moment, the load-deflection curve $\Delta(P)$ at the unit load point can be calculated using the virtual work principle, as defined in Eq. (62).

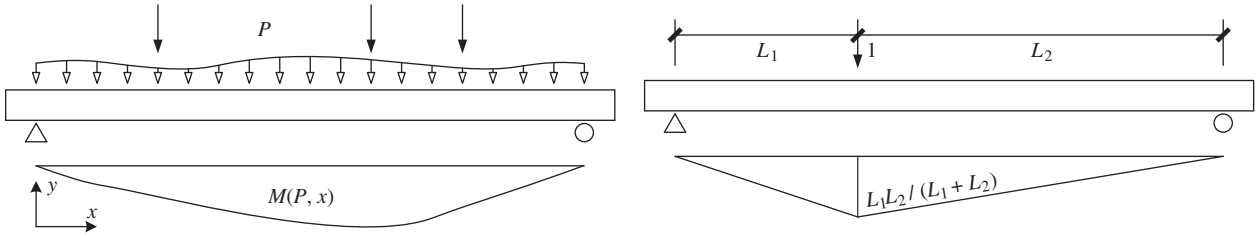

(a) (b)

Figure 10: Bending moment diagram of external loads and unit load. (a) External load and (b) Unit load

$$\Delta(P) = \int_0^L \overline{M}(x)k[M(P,x)]\mathrm{d}x \tag{62}$$

where $k[M(P,x)]$ refers to the relationship between the curvature and bending moment. The curvature k is a function of bending moment M.

Fig. 11 shows the calculation process of the load-deflection curves. There are three steps in the calculation. For a single-pole bamboo beam, 1) The maximum bending moment of the elastic stage M_p and the ultimate bending moment M_u should be solved. Two bending moments are adopted to differentiate the elastic stage, elastic-plastic stage, and failure stage. 2) When a bending moment M is

given, the stage can be determined. Then, the curvature k is calculated for the corresponding stage. Based on the previous analysis, a function for calculating curvature k has been established, where the bending moment M is an independent variable. 3) Finally, the moment diagram $M(P, x)$, induced by external load P, is plotted. The load-deflection curve $\Delta(P)$ can be calculated using Eq. (62).

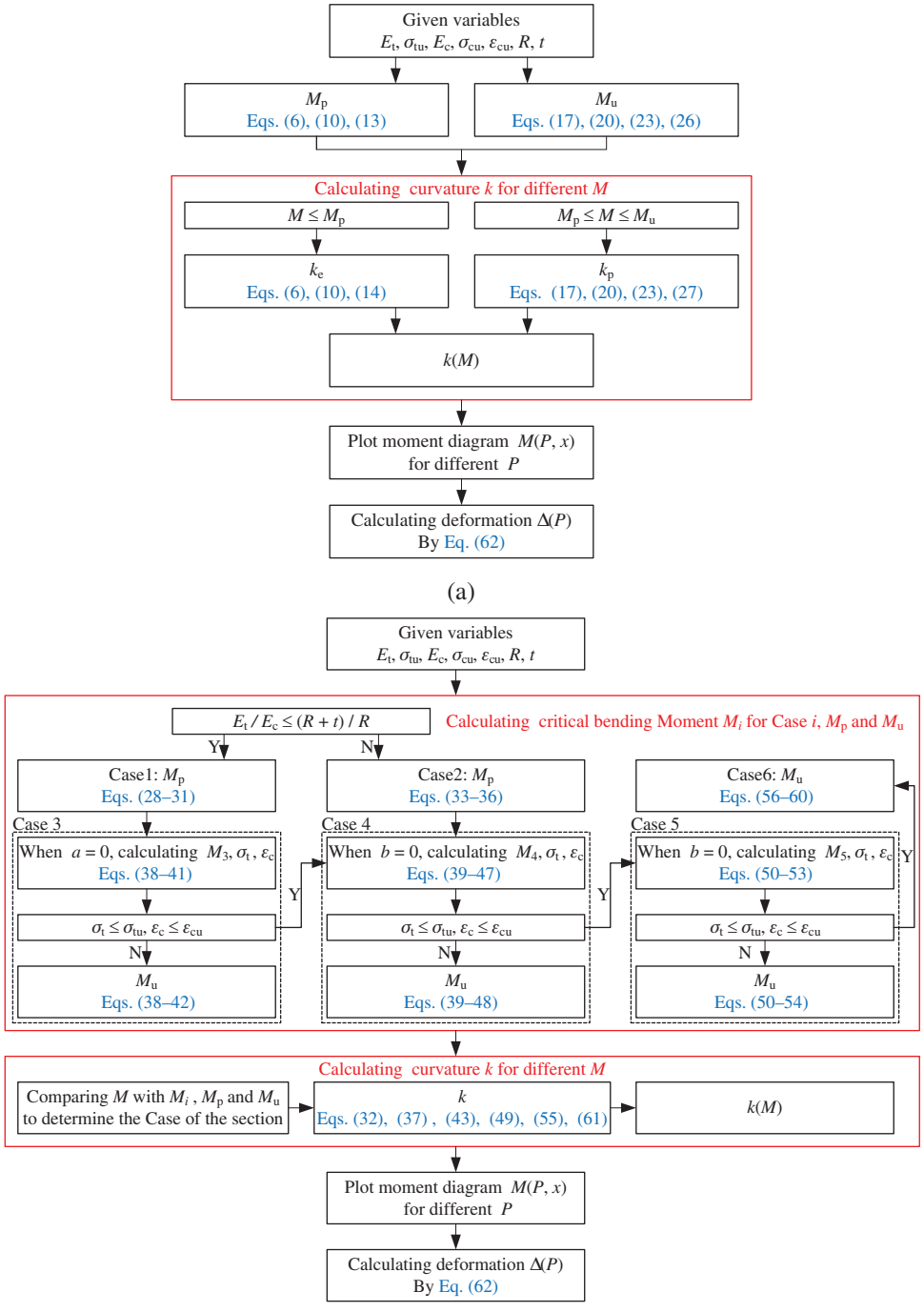

Figure 11: Calculation process of load-deflection curves. (a) Single-pole bamboo beam and (b) Double-pole bamboo beam

The elastic stage of a double-pole bamboo beam can be considered for two cases and the elastic-plastic stage for four. For this reason, the first two steps for a double-pole bamboo beam are more complicated. However, the load-deflection curve calculations are the same as for a single-pole bamboo beam. The critical bending moment M_i is the maximum bending moment of case i in the elastic-plastic stage. It is utilized to differentiate four cases in the elastic-plastic stage. The solution for M_p contains two types of conditions that correspond to two cases of the elastic stage. Failure in the elastic-plastic stage may occur in one of four cases; thus, the solution of M_u includes four types of conditions.

2.5 Influence of Interfacial Slippage

The interfacial slippage between two bamboo poles is difficult to avoid; this has not been previously considered in double-pole bamboo beam analyses. The influence of interfacial slippage is analyzed based on the following assumptions: 1) The bamboo materials are linearly elastic. 2) The shear force at the interface is proportional to the slippage. 3) The curvatures and deflections of the two bamboo poles are consistent. 4) The shear deformation is not considered when the plane-section assumption is satisfied.

Fig. 12 shows an interfacial slippage diagram. The equilibrium differential equation, based on a tiny segment, is presented in Eq. (63). When the boundary conditions are imported, the interfacial slippage u can be solved. For simply supported and free ends, $u' = 0$; for a fixed end and symmetric section, $u = 0$. Then, the extra curvature k_s caused by the interfacial slippage can be calculated using Eq. (66). The extra curvature k_s is a function of the vertical shear force V. Ultimately, Eq. (67) provides the method for solving the extra deflection $\Delta_s(P)$ caused by interfacial slippage.

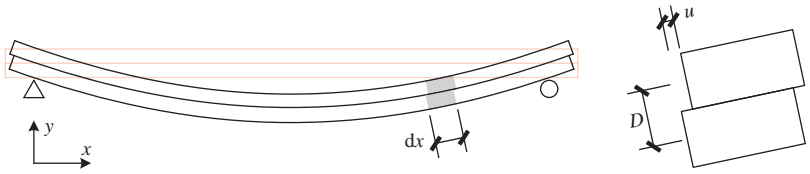

Figure 12: Interfacial slippage diagram

$$u'' - \alpha^2 u = VD/EI_0 \tag{63}$$

$$\alpha^2 = \frac{KD^2}{EI_0(1 - EI_0/EI_\infty)} \quad D = 2R + t \tag{64}$$

$$EI_\infty = EI_0 + EAD^2 \quad EI_0 = E_1I_1 + E_2I_2 \quad 1/EA = 1/E_1A_1 + 1/E_2A_2 \tag{65}$$

$$k_s = (1 - EI_0/EI_\infty)u'/D \tag{66}$$

$$\Delta_s(P) = \int_0^L \overline{M} k_s[V(P,x)]\mathrm{d}x \tag{67}$$

where D represents the distance of the horizontal symmetry axes in the two bamboo poles. K is the shear stiffness of the interface per unit length. For simplification, the difference in the elastic modulus is not considered in the tensile and compressive states. The influence of not considering the difference can be ignored, which will be demonstrated in the following analysis. E_1 and E_2 are the elastic moduli of the top and bottom bamboo poles, respectively, i.e., the mean value of E_t and E_c. I_1 and I_2 represent the moments of inertia and A_1 and A_2 represent the sectional areas.

3 FE Analysis of Bamboo Beams

3.1 Single-Pole Bamboo Beam

FE analysis was adopted to validate the above analysis. Fig. 13a manifests the two-point loading pattern that is recommended for bending tests on bamboo [1]. This two-point loading pattern was adopted to conduct a case study of bamboo beams. The bending moment diagram of two-point loading is similar to that of a uniform load. To calculate the midspan deflection, Fig. 13(b) displays the bending moment diagram of the midspan unit load.

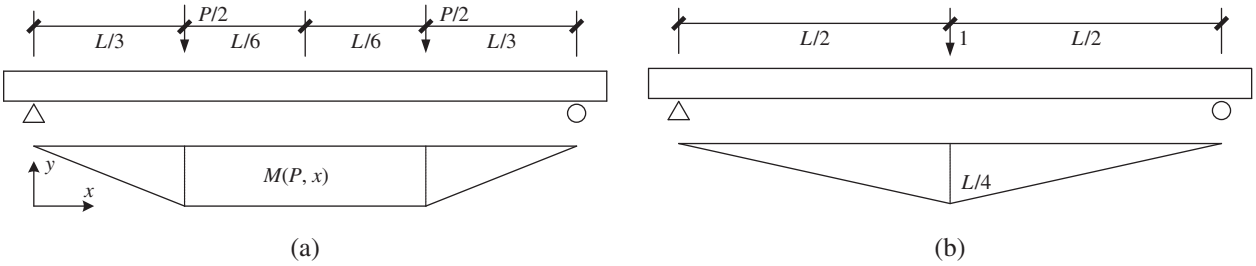

Figure 13: Bending moment diagram of two-point loading and midspan unit load. (a) Two-point loading and (b) Midspan unit load

Fig. 14 presents the FE model of a single-pole bamboo beam, using the method presented in the literature [38]. The span was 3 m and the section size was Φ100 × 8 mm. Coupling was used at two loading points and two support points. The solid element C3D8R was employed. The overall mesh size was 16 mm while the mesh size in the thickness direction was 4 mm. The properties of the bamboo are listed in Tab. 1. The different elastic moduli in the tensile and compressive states could not be simulated in the FE model. Therefore, the mean values of E_t and E_c were applied. Based on the original model, two additional FE models that consider the taper and bamboo joints were developed. The taper was 0.6% and the thickness of the bamboo joints was 8 mm. The properties of the joints are consistent with those of bamboo. The joints were tied to the internal surface at intervals of 300 mm. In addition, single-pole bamboo beams with spans of 4.5 m and 6 m were simultaneously analyzed.

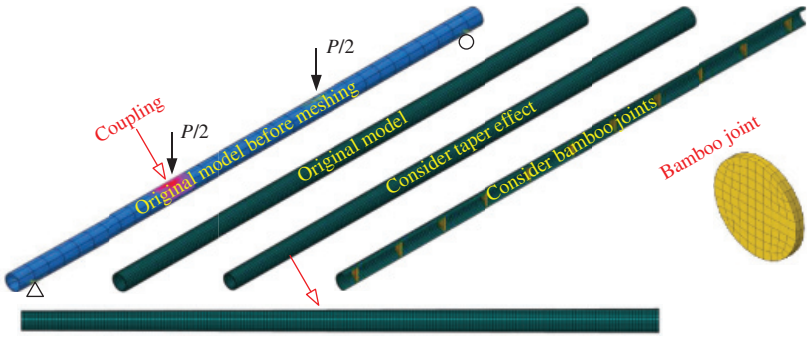

Figure 14: FE model of a single-pole bamboo beam

Table 1: Properties of the bamboo [23]

E_t/GPa	E_c/GPa	σ_{tu}/MPa	σ_{cu}/MPa	ε_{cu}
13	12	180	60	0.02

Fig. 15 compares the theoretical and FE results for a single-pole bamboo beam. When the difference in the elastic modulus is not considered, the load-deflection curves can be calculated from theoretical analysis (the 'Theory-Simplify' curves in Fig. 15). These match well with the theoretical load-deflection curves when the difference is considered. Consequently, the mean values of E_t and E_c are utilized in the FE analysis.

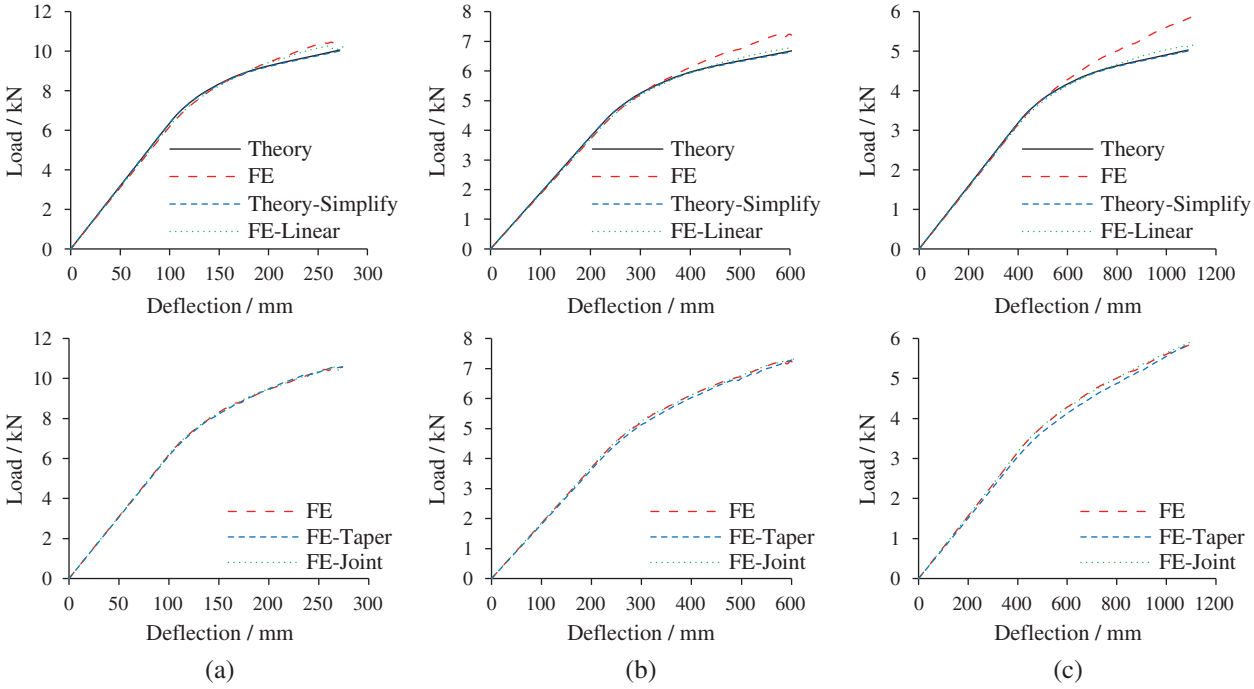

Figure 15: Comparison of theoretical and FE results for single-pole bamboo beams. (a) L = 3 m, (b) L = 4.5 m and (c) L = 6 m

During the initial stage, the FE results are consistent with the theoretical results. However, there are some discrepancies in the large deformation stage. The load-deflection curves (referred to as FE-Linear because the FE model is analyzed without considering geometric nonlinearities) almost coincide with the theoretical results, indicating that the discrepancy is caused by geometric nonlinearity. The effect of tapering and joints along the length of the bamboo beam is limited. Considering these two factors improves the similarity between the load-deflection curves and original model.

Fig. 16 shows the ultimate state of single-pole bamboo beams with a span of 3 m. The neutral axis moves downward due to the greater tensile strength. When the geometric nonlinearity is not considered, the horizontal displacement of the support points is negligible. After considering the taper, the deformation is asymmetric and the maximum stress occurs on the left side with a smaller section size. The stress and deformation distributions when considering the bamboo joint are the same as those of the original model.

3.2 Double-Pole Bamboo Beam without Interfacial Slippage

Fig. 17 depicts the FE model of a double-pole bamboo beam. The modeling strategy was identical to that of a single-pole bamboo beam. The axial connector was adopted to simulate the tangential interaction of the top and bottom bamboo poles. The normal interaction was determined as a hard contact. Two bamboo poles were evenly divided into thirty sections along the axis and thirty connectors were installed. For different spans, each connector joined different beam lengths. When the spans were 3 m, 4.5 m, and 6 m, the connected lengths l were 100 mm, 150 mm, and 200 mm, respectively. Coupling was used to link the

connector and corresponding parts. Two bamboo poles in the FE model were placed in opposite directions to negate the poles' taper. The bamboo joints in the top and bottom bamboo poles were evenly distributed along the axis. To investigate the flexural behavior of a double-pole bamboo beam without slippage, the stiffness of the axis connectors was set as infinite.

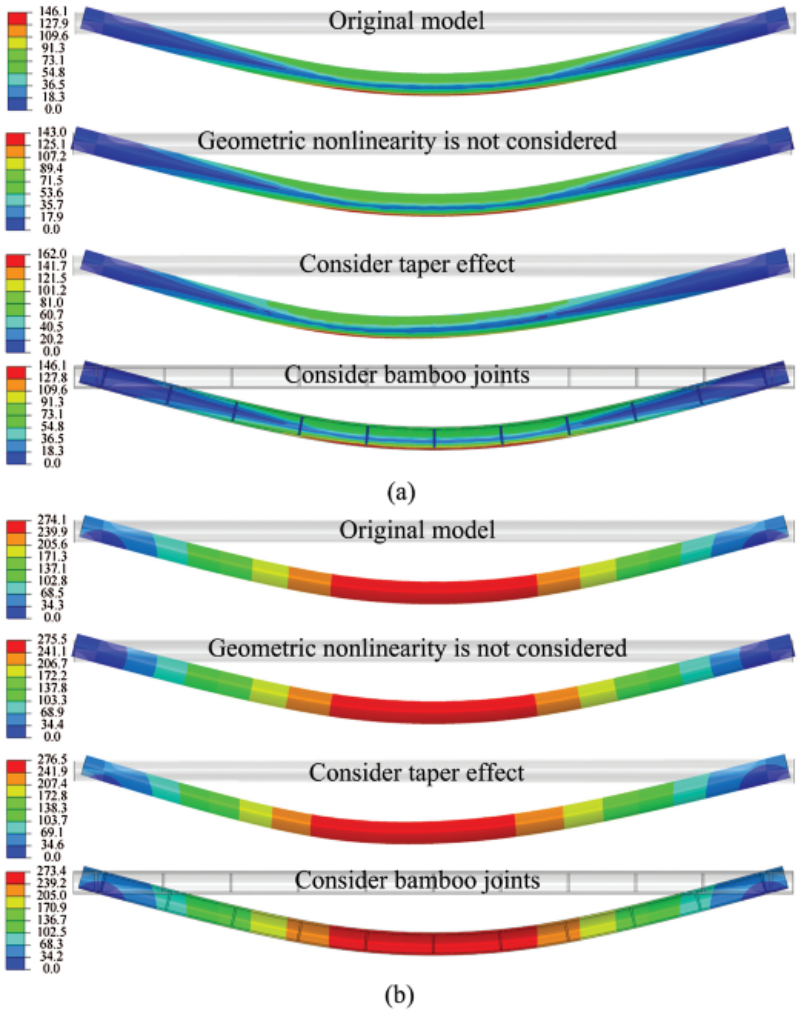

Figure 16: Ultimate state of single-pole bamboo beams (L = 3 m). (a) Stress distribution (Unit: MPa) and (b) Deformation distribution (Unit: mm)

Fig. 18 compares the theoretical and FE results for a double-pole bamboo beam. The FE results match well with the theoretical results Eqs. (63)–(67). The deformation capacity of single-pole bamboo beams is twice that of double-pole bamboo beams. Therefore, the influence of geometric nonlinearity is not obvious in double-pole bamboo beams. Owing to the reverse placement of two poles, the influence of the taper is reduced.

Fig. 19 displays the ultimate state of double-pole bamboo beams with a span of 3 m. Interfacial slippage is not observed in the four FE models and the neutral axis moves downward. The horizontal displacement of the support points is small and the influence of geometric nonlinearity is restricted. The stress and deformation distributions also illustrate that the taper has little effect on the flexural behavior of double-pole bamboo beams.

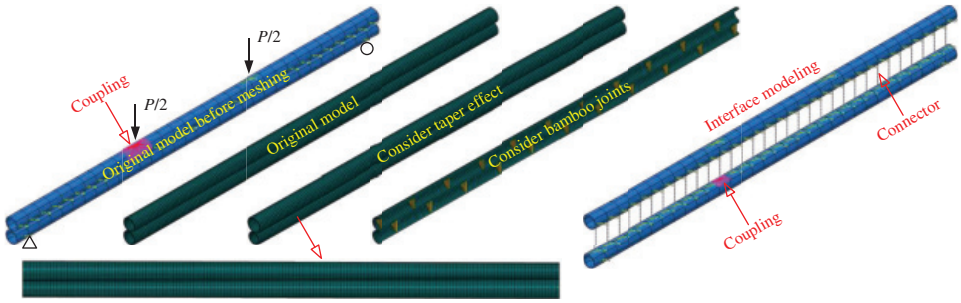

Figure 17: FE model of a double-pole bamboo beam

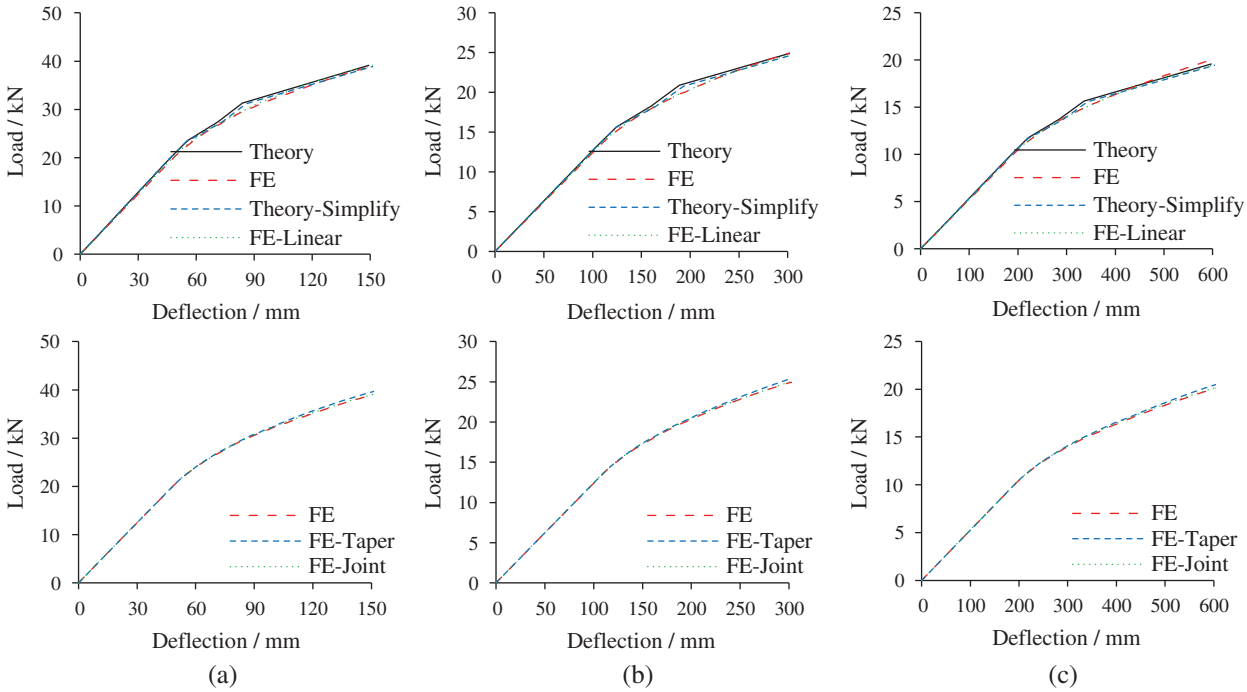

Figure 18: Comparison of theoretical and FE results for double-pole bamboo beams. (a) L = 3 m, (b) L = 4.5 m and (c) L = 6 m

3.3 Double-Pole Bamboo Beam with Interfacial Slippage

The theoretical analysis of the interfacial slippage is only suitable for the elastic stage [39–41]. The FE analysis can compensate for this. Four FE models, with different connector stiffnesses S, were established. The individual stiffnesses were set as 6.4 kN/mm, 1.6 kN/mm, 0.4 kN/mm, and 0 kN/mm. Fig. 20 depicts the load-deflection curves with interfacial slippage. The FE results agree well with the theoretical results in the elastic stage. The connector stiffness S has a significant influence on the flexural behavior of double-pole bamboo beams. When the stiffness is 6.4 kN/mm, the load-deflection curve is close to that when slippage is not considered. The shear stiffness of the interface per unit length K is the ratio of the connector stiffness S to the connected length l (Eq. (68)). Thus, the K requirement decreases with increasing span.

$$K = S/l \tag{68}$$

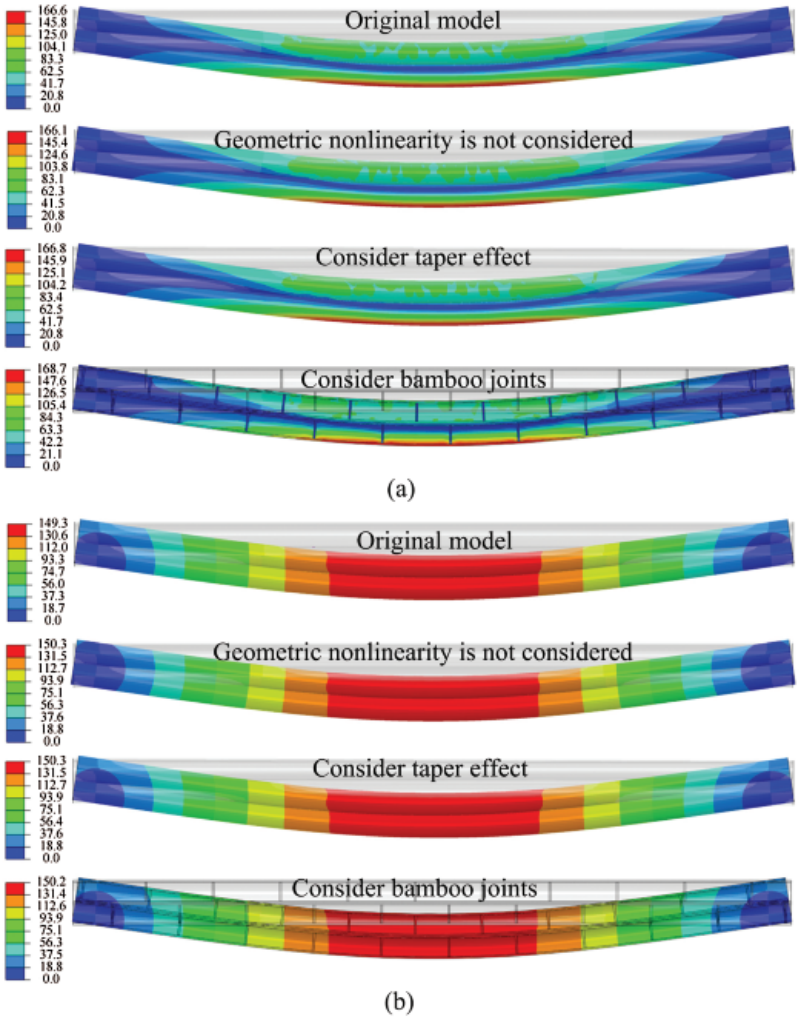

Figure 19: Ultimate state of double-pole bamboo beams (L = 3 m). (a) Stress distribution (Unit: MPa) and (b) Deformation distribution (Unit: mm)

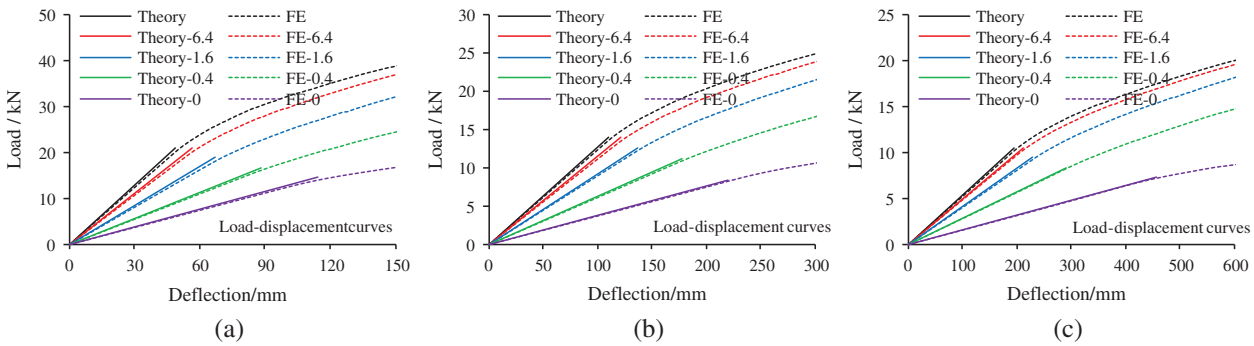

Figure 20: Load-deflection curves with interfacial slippage. (a) L = 3 m, (b) L = 4.5 m and (c) L = 6 m

Fig. 21 compares the slippage distribution of double-pole bamboo beams in the elastic stage. The theoretical analysis of interfacial slippage proves to be correct and reasonable. The slippage is

concentrated at the beam ends. With increasing connector stiffness, the interfacial slippage gradually decreases. Fig. 22 shows the interfacial shear force of the double-pole bamboo beams when the connector stiffness is 6.4 kN/mm. The interfacial shear force is equal to the axial force on the connectors. Considering symmetry, only the axial force of the fifteen connectors on the left side of the bamboo beam are presented. The connectors are numbered from left to right. Connector 1 is near the left support point and the axial force there is the greatest. Fig. 23 displays the ultimate states of the double-pole bamboo beams when the connector stiffness is 0 kN/mm. Two neutral axes are observed in the top and bottom bamboo poles. The stress distribution is similar to that of a single-pole bamboo beam. Significant interfacial slippages are observed at both ends of the double-pole bamboo beams.

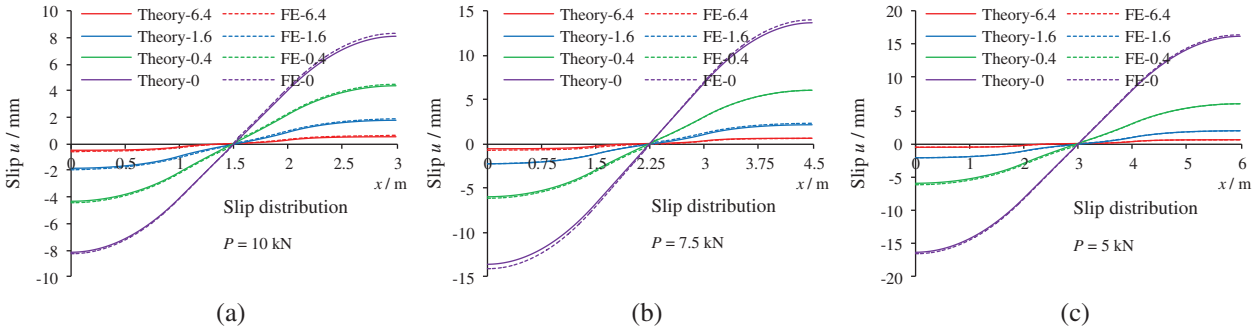

Figure 21: Slippage distribution of the double-pole bamboo beams. (a) L = 3 m, (b) L = 4.5 m and (c) L = 6 m

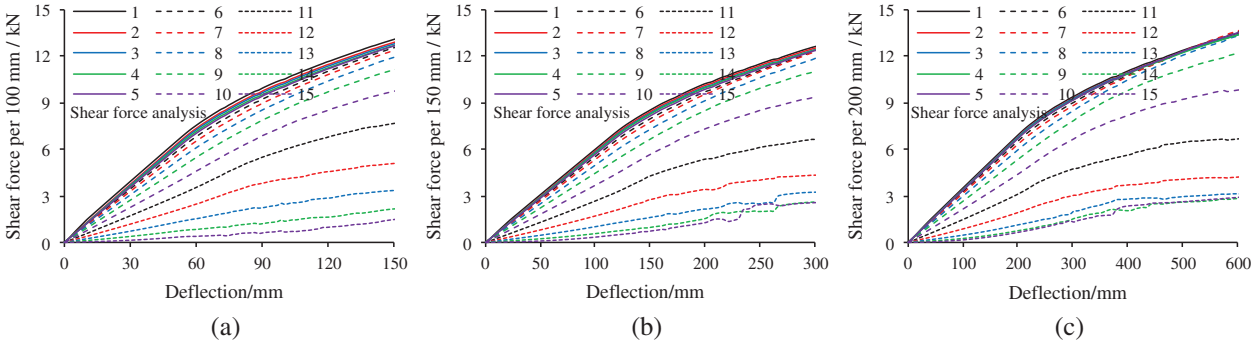

Figure 22: Shear force analysis of the double-pole bamboo beams. (a) L = 3 m, (b) L = 4.5 m and (c) L = 6 m

3.4 Novel Configuration to Avoid Slippage

Fig. 24 proposes a novel configuration to avoid slippage. Two bamboo poles are bound together using diagonal steel bands. The inclination of the steel band conforms to the direction of slippage. Owing to the diagonal arrangement, the tension stiffness of the steel bands is converted to horizontal shear stiffness between the two bamboo poles. The top and bottom areas of the steel band compressing the bamboo poles should be firmly fixed to the poles. Structural adhesives and pneumatic nails are two recommended methods. The methods should not damage the poles [24,25].

The diagonal steel bands should meet the two requirements of stiffness and strength. Fig. 25 shows the stiffness of a single diagonal steel band S, which can be calculated using Eq. (69). The ultimate bearing capacity of the steel band F_u is also deduced using Eq. (70). Moreover, the quantity of steel in the diagonal area m is an important economic consideration, as shown in Eq. (71), since it contributes to the cost of these measures.

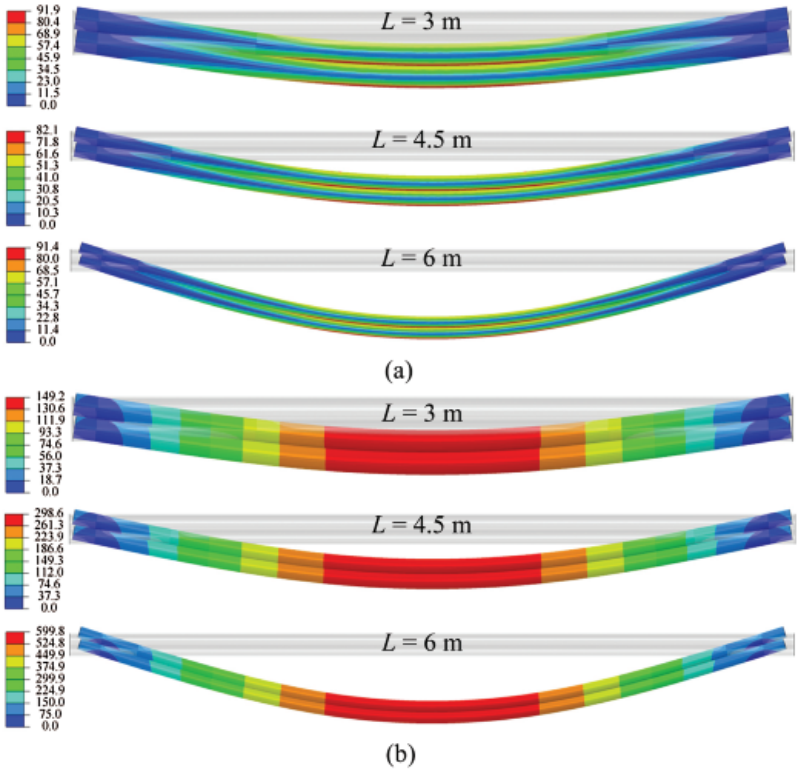

Figure 23: Ultimate state of double-pole bamboo beams with interfacial slippage. (a) Stress distribution (Unit: MPa) and (b) Deformation distribution (Unit: mm)

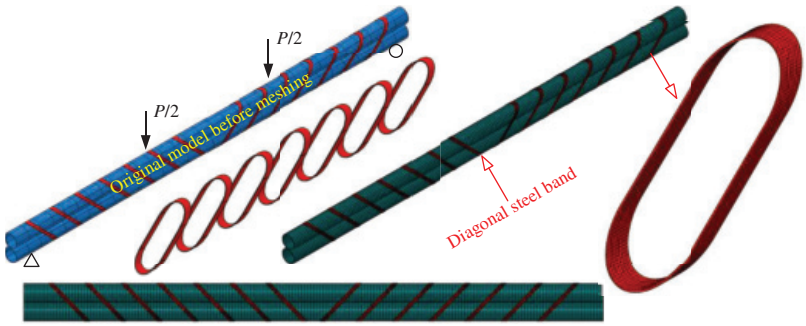

Figure 24: FE model of a double-pole bamboo beam with diagonal steel bands (L = 3 m)

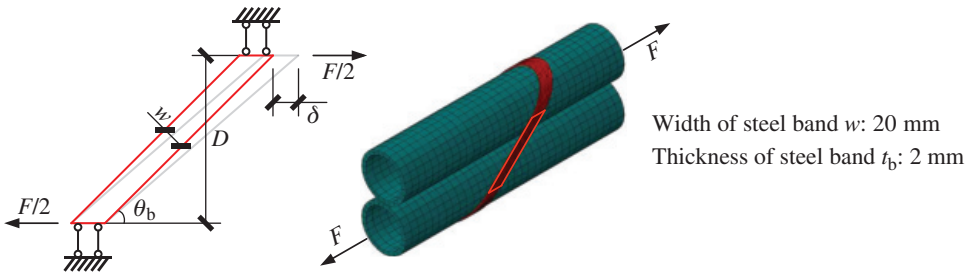

Figure 25: Mechanical diagram and FE model of a single diagonal steel band

$$S = F/\delta = 2E_b w t_b \cos^2\theta_b \sin\theta_b / D \tag{69}$$

$$F_u = 2 f_y w t_b \cos\theta_b \tag{70}$$

$$m = 2 w t_b D / \sin\theta_b \tag{71}$$

where E_b and f_y are the elastic modulus and yield stress of the steel band, respectively. w and t_b represent the width and thickness of the band, respectively. θ_b refers to the inclination angle.

The steel band cannot be sufficiently broad for the shear deformation to cause uneven stretching. Thus, a steel band width of 20 mm is suggested. The thickness of 2 mm is decided to facilitate fabrication. An ideal elastic-plastic constitutive model is adopted for the following analysis and the yield stress of the steel band is 235 MPa. Fig. 26 shows the results of the theoretical analysis. The ratio of S to m and the ratio of F_u to m are greatest when the inclination angle θ_b is 45°. Thus, it is cost-effective for θ_b to be 45°. At this moment, the stiffness of a single diagonal steel band S is 58.3 kN/mm and the ultimate bearing capacity F_u is 13.3 kN. Fig. 27 presents the FE results of a single diagonal steel band, which agree well with those of the theoretical analysis.

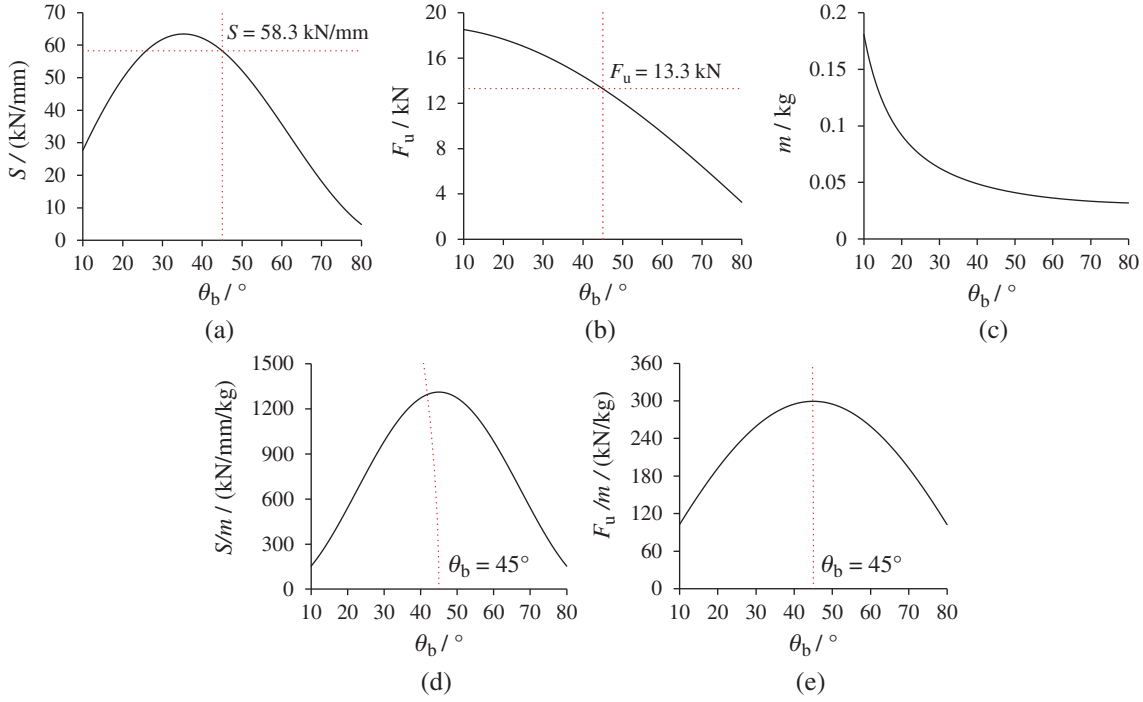

Figure 26: Results of theoretical analysis for a single diagonal steel band. (a) $S - \theta_b$, (b) $F_u - \theta_b$, (c) $m - \theta_b$, (d) $S/m - \theta_b$ and (e) $F_u/m - \theta_b$

The steel band combined with bamboo is also simulated. The FE model is illustrated in Fig. 25. The length of the bamboo sample is 500 mm, which is sufficient to analyze the stiffness of the diagonal steel band in working conditions. The steel band is attached to the top and bottom surfaces of the bamboo. A shell element, S4R, with a mesh size of 4 mm, is implemented for the steel band. Fig. 27 presents the FE results. The stiffness S decreases to 10.4 kN/mm due to the bamboo's deformation. The ultimate bearing capacity F_u is slightly affected and remains almost unchanged. These are the application parameters for diagonal steel bands.

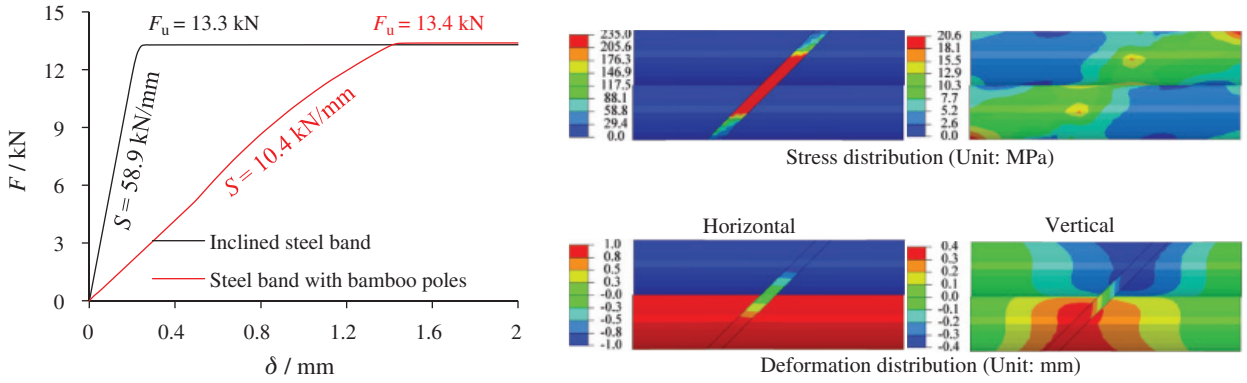

Figure 27: FE results of a single diagonal steel band

Based on the model FE-0, a double-pole bamboo beam with diagonal steel bands is assembled, as shown in Fig. 24. The spacing of the diagonal steel bands is equivalent to the connected length l, which is set to 200 mm in Fig. 24. The modeling strategy for the steel bands is identical to that in Fig. 25. Meanwhile, the FE models with different spacings are simulated, presented in Tab. 2. The spacing enlarges as the span increases. Fig. 28 compares the load-deflection curves. Note that the ultimate load and displacement are smaller than those of the FE model without steel bands. Fig. 29 shows the ultimate state of the model with steel bands, demonstrating that the steel band yielded completely and is not fastened to the bamboo poles.

Table 2: Details of a double-pole bamboo beam with diagonal steel bands

L/m	Case	l/mm	S/(kN/mm)	K/(N/mm^2)	F_u/kN	F_u/l/(N/mm)
3	FE	100	∞	∞	∞	∞
	FE-6.4	100	6.4	64	∞	∞
	Steel band-400	400		26		33.5
	Steel band-200	200	10.4	52	13.4	67
	Steel band-100	100		104		134
4.5	FE	150	∞	∞	∞	∞
	FE-6.4	150	6.4	42.7	∞	∞
	Steel band-600	600		17.3		22.3
	Steel band-300	300	10.4	34.7	13.4	44.7
	Steel band-150	150		69.3		89.3
6	FE	200	∞	∞	∞	∞
	FE-6.4	200	6.4	32	∞	∞
	Steel band-800	800		13		16.8
	Steel band-400	400	10.4	26	13.4	33.5
	Steel band-200	200		52		67

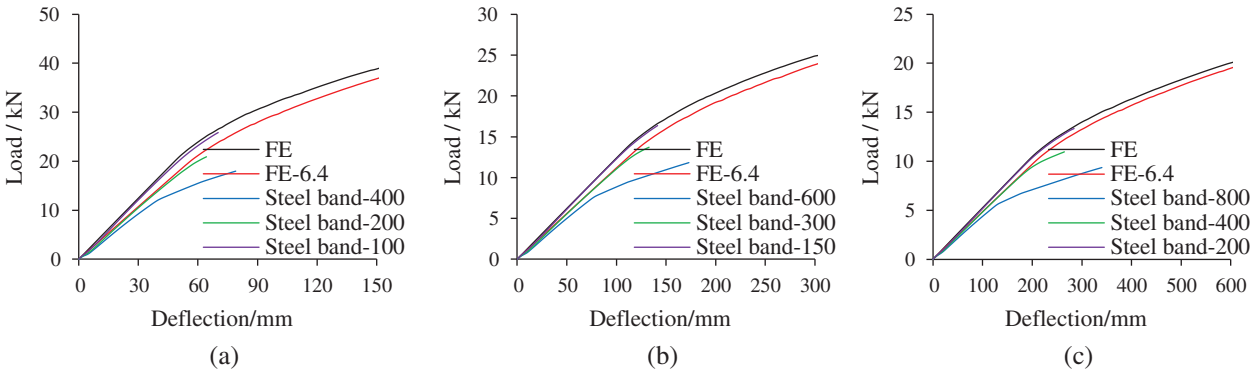

Figure 28: Load-deflection curves with diagonal steel bands. (a) L = 3 m, (b) L = 4.5 m and (c) L = 6 m

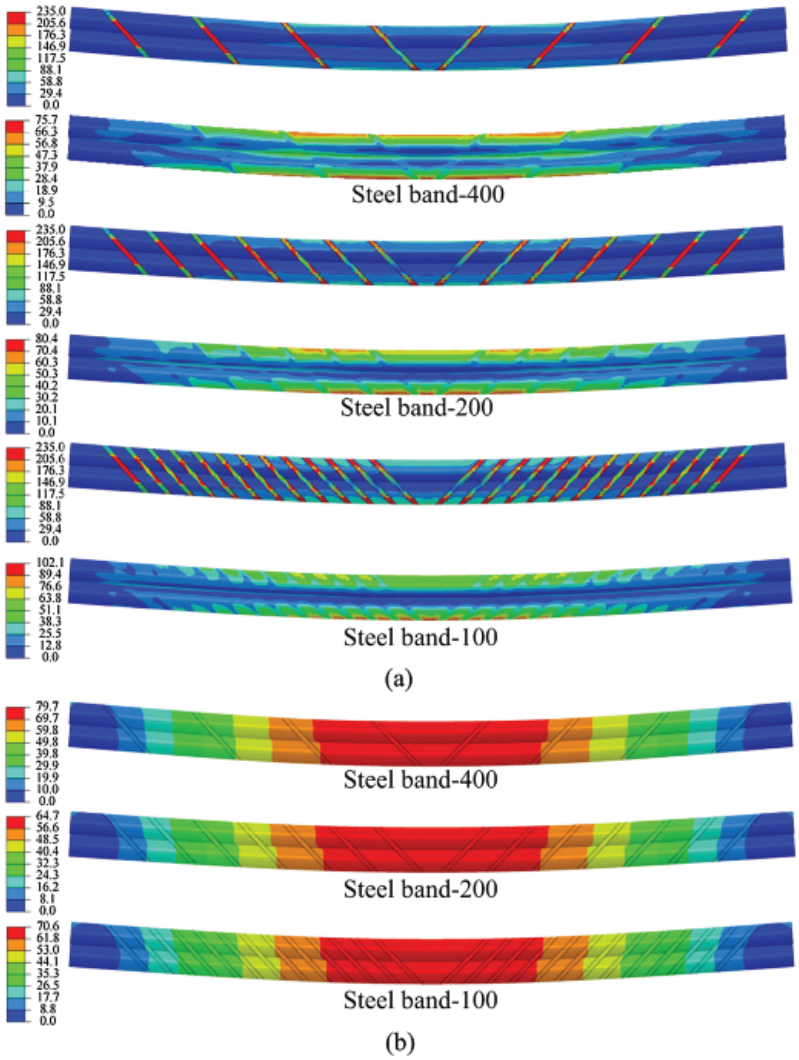

Figure 29: Ultimate state of double-pole bamboo beams with diagonal steel bands (L = 3 m). (a) Stress distribution (Unit: MPa) and (b) Deformation distribution (Unit: mm)

When the span is 3 m and the spacing is 100 mm, the interfacial slippage can be restrained. Its load-deflection curve is consistent with that of the FE model without slippage. The shear stiffness of the interface per unit length K is 104 N/mm^2, which is greater than that of FE-6.4. As shown in Fig. 22, it is sufficient that the ultimate bearing capacity of the steel band F_u is 13.4 kN. To reduce costs, the spacing should be increased to 200 mm. The initial slope of the load-deflection curve only reduces by 13.9%. A spacing of 200 mm is recommended when the span is 3 m. In this case, K is 52 N/mm^2, which is close to that of FE-6.4.

4 Conclusions

In this study, the flexural behavior of single-pole and double-pole bamboo beams was investigated via theoretical analysis. Simultaneously, the influence of interfacial slippage was analyzed. Then, an effective configuration to avoid slippage was proposed and validated. The following conclusions can be drawn:

1. A method for calculating the load-deflection curve is proposed, considering the material's nonlinearity. FE analysis is conducted to validate the calculation method. The FE results match well with the theoretical results. Moreover, the FE results indicate that the influences of the poles' natural taper and bamboo joints are limited.
2. The interfacial slippage between the two bamboo poles is difficult to avoid in double-pole bamboo beams. The shear stiffness of the interface per unit length has a significant influence on the flexural behavior of double-pole bamboo beams. For different shear stiffnesses, the load-deflection curves are obtained via theoretical and FE analyses.
3. A novel configuration using diagonal steel bands is presented to avoid slippage. Owing to the diagonal arrangement, the tension stiffness of the steel band can be converted to horizontal shear stiffness between the two bamboo poles. An inclination angle of 45° is suggested to adequately develop the stiffness and bearing capacity of the band.

Funding Statement: This research was supported by the National Key Research and Development Program of China (Grant No. 2017YFC0703502), the National Natural Science Foundation of China (Grant No. 51608433), the Key Lab of Plateau Building and Eco-Community in Qinghai (KLKF-2020-001), and the Shaanxi Province Youth Science and Technology New Star Program (Grant No. 2019KJXX-040). These financial supports are greatly acknowledged.

Conflicts of Interest: The authors declare that they have no conflicts of interest to report regarding the present study.

References

1. International Organization for Standardization (2004). *ISO 22157-1-2004. Bamboo–Determination of physical and mechanical properties–Part 1: Requirements*. Geneva, Switzerland.
2. Tian, L. M., Jin, B. B., Hao, J. P. (2019). Research and application of modern bamboo structures. *Engineering Mechanics, 36(5),* 1–18.
3. García, J. J., Rangel, C., Ghavami, K. (2012). Experiments with rings to determine the anisotropic elastic constants of bamboo. *Construction and Building Materials, 31,* 52–57. DOI 10.1016/j.conbuildmat.2011.12.089.
4. Akinbade, Y., Harries, K. A., Flower, C. V., Nettleship, I., Papadopoulos, C. et al. (2019). Through-culm wall mechanical behaviour of bamboo. *Construction and Building Materials, 216(1),* 485–495. DOI 10.1016/j.conbuildmat.2019.04.214.
5. Liu, P. C., Zhou, Q. S., Jiang, N., Zhang, H., Tian, J. F. (2020). Fundamental research on tensile properties of phyllostachys bamboo. *Results in Materials, 7,* 100076. DOI 10.1016/j.rinma.2020.100076.
6. Qiu, Z. Y., Fan, H. L. (2020). Nonlinear modeling of bamboo fiber reinforced composite materials. *Composite Structures, 238(1),* 111976. DOI 10.1016/j.compstruct.2020.111976.

7. Chung, K. F., Yu, W. K. (2002). Mechanical properties of structural bamboo for bamboo scaffoldings. *Engineering Structures, 24(4),* 429–442. DOI 10.1016/S0141-0296(01)00110-9.
8. Albermani, F., Goh, G. Y., Chan, S. L. (2007). Lightweight bamboo double layer grid system. *Engineering Structures, 29(7),* 1499–1506. DOI 10.1016/j.engstruct.2006.09.003.
9. Paraskeva, T. S., Grigoropoulos, G., Dimitrakopoulos, E. G. (2017). Design and experimental verification of easily constructible bamboo footbridges for rural areas. *Engineering Structures, 143(9),* 540–548. DOI 10.1016/j.engstruct.2017.04.044.
10. Villegas, L., Morán, R., García, J. J. (2019). Combined culm-slat Guadua bamboo trusses. *Engineering Structures, 184(2),* 495–504. DOI 10.1016/j.engstruct.2019.01.114.
11. Tian, L. M., Kou, Y. F., Hao, J. P. (2019). Axial compressive behaviour of sprayed composite mortar–original bamboo composite columns. *Construction and Building Materials, 215(9),* 726–736. DOI 10.1016/j.conbuildmat.2019.04.234.
12. Bahtiar, E. T., Malkowska, D., Trujillo, D., Nugroho, N. (2021). Experimental study on buckling resistance of Guadua angustifolia bamboo column. *Engineering Structures, 228,* 111548. DOI 10.1016/j.engstruct.2020.111548.
13. Sá Ribeiro, R. A., Sá Ribeiro, M. G., Miranda, I. P. A. (2017). Bending strength and nondestructive evaluation of structural bamboo. *Construction and Building Materials, 146(1),* 38–42. DOI 10.1016/j.conbuildmat.2017.04.074.
14. García-Aladín, M. F., García, H., Mosquera, L. M., García, J. J. (2014). The importance of shear in the deflection of bamboo beams. *Key Engineering Materials, 600,* 87–96. DOI 10.4028/www.scientific.net/KEM.600.87.
15. García-Aladín, M. F., García, J. J., Correal, J. F. (2018). Theoretical and experimental analysis of two-culm bamboo beams. *Proceedings of the Institution of Civil Engineers-Structures and Buildings, 171(4),* 316–325. DOI 10.1680/jstbu.16.00044.
16. Trujillo, D., Jangra, S., Gibson, J. M. (2016). Flexural properties as a basis for bamboo strength grading. *Proceedings of the Institution of Civil Engineers-Structures and Buildings, 170(4),* 1–12.
17. Nurmadina, Nugroho, N., Bahtiar, E. T. (2017). Structural grading of Gigantochloa apus bamboo based on its flexural properties. *Construction and Building Materials, 157(1),* 1173–1189. DOI 10.1016/j.conbuildmat.2017.09.170.
18. Lorenzo, R., Mimendi, L., Li, H. T., Yang, D. (2020). Bimodulus bending model for bamboo poles. *Construction and Building Materials, 262(2),* 120876. DOI 10.1016/j.conbuildmat.2020.120876.
19. European Committee for Standardization (2004). *EN 1995-1-1, Eurocode 5: Design of timber structures–Part 1-1: General–Common rules and rules for buildings*. Brussels, Belgium.
20. Standardization Administration of China (2003). *GB 50005-2003. Code for design of timber structures*. Beijing, China.
21. Zhang, T. C., Wang, A. L., Wang, Q. S., Guan, F. R. (2019). Bending characteristics analysis and lightweight design of a bionic beam inspired by bamboo structures. *Thin-Walled Structures, 142(3),* 476–498. DOI 10.1016/j.tws.2019.04.043.
22. Zhang, T. C., Duan, C. M., Wang, A. L., Wang, Q. S. (2020). Dynamic modeling and optimal design of Tube–Diaphragm coupling beam inspired by bamboo. *Thin-Walled Structures, 155,* 106836. DOI 10.1016/j.tws.2020.106836.
23. Tian, L. M., Kou, Y. F., Hao, J. P. (2019). Flexural behavior of sprayed lightweight composite mortar-original bamboo composite beams: Experimental study. *Bioresources, 14(1),* 500–517.
24. Villegas, L., Moran, R., Muñoz, J., García, J. J. (2019). Combined culm-slat Guadua bamboo trusses. *Engineering Structures, 184(2),* 495–504. DOI 10.1016/j.engstruct.2019.01.114.
25. García, J. J., Moran, R. (2019). Bamboo joints with steel clamps capable of transmitting moment. *Construction and Building Materials, 216(1),* 249–260. DOI 10.1016/j.conbuildmat.2019.05.025.
26. Villegas, L., Moran, R., Muñoz, J., García, J. J. (2015). A new joint to assemble light structures of bamboo slats. *Construction and Building Materials, 98,* 61–68. DOI 10.1016/j.conbuildmat.2015.08.113.

27. Wang, F. L., Yang, J. (2020). Experimental and numerical investigations on load-carrying capacity of dowel-type bolted bamboo joints. *Engineering Structures, 209,* 109952. DOI 10.1016/j.engstruct.2019.109952.
28. Mouka, T., Dimitrakopoulos, E. G. (2021). Simulation of embedment phenomena on bamboo culms via a modified foundation modelling approach. *Construction and Building Materials, 275(7),* 122048. DOI 10.1016/j.conbuildmat.2020.122048.
29. Sharma, B., Gatoo, A., Bock, M., Ramage, M. H. (2015). Engineered bamboo for structural applications. *Construction and Building Materials, 81(2),* 66–73. DOI 10.1016/j.conbuildmat.2015.01.077.
30. Sun, X. F., He, M. J., Li, Z. (2020). Novel engineered wood and bamboo composites for structural applications: State-of-art of manufacturing technology and mechanical performance evaluation. *Construction and Building Materials, 249(6780),* 118751. DOI 10.1016/j.conbuildmat.2020.118751.
31. Huang, D. S., Zhou, A. P., Bian, Y. L. (2013). Experimental and analytical study on the nonlinear bending of parallel strand bamboo beams. *Construction and Building Materials, 44(5),* 585–592. DOI 10.1016/j.conbuildmat.2013.03.088.
32. Li, H. T., Wu, G., Zhang, Q. S., Deeks, A. J., Su, J. W. (2018). Ultimate bending capacity evaluation of laminated bamboo lumber beams. *Construction and Building Materials, 160(4),* 365–375. DOI 10.1016/j.conbuildmat.2017.11.058.
33. Wei, Y., Ji, X. W., Duan, M. J., Li, G. F. (2017). Flexural performance of bamboo scrimber beams strengthened with fiber-reinforced polymer. *Construction and Building Materials, 142(2),* 66–82. DOI 10.1016/j.conbuildmat.2017.03.054.
34. Wang, Z. Y., Wei, Y., Li, N., Zhao, K., Ding, M. M. (2020). Flexural behavior of bamboo-concrete composite beams with perforated steel plate connections. *Journal of Wood Science, 66(4),* 1–20. DOI 10.1186/s10086-020-1848-7.
35. Zhong, Y., Wu, G. F., Ren, H. Q., Jiang, Z. H. (2017). Bending properties evaluation of newly designed reinforced bamboo scrimber composite beams. *Construction and Building Materials, 143(1),* 61–67. DOI 10.1016/j.conbuildmat.2017.03.052.
36. Wei, Y., Yan, S. C., Zhao, K., Dong, F. H., Li, G. F. (2020). Experimental and theoretical investigation of steel-reinforced bamboo scrimber beams. *Engineering Structures, 223,* 111179. DOI 10.1016/j.engstruct.2020.111179.
37. Li, Y. S., Shan, W., Shen, H. Y., Zhang, Z. W., Liu, J. Z. (2015). Bending resistance of I-section bamboo–steel composite beams utilizing adhesive bonding. *Thin-Walled Structures, 89(5),* 17–24. DOI 10.1016/j.tws.2014.12.007.
38. Akinbade, Y., Nettleship, I., Papadopoulos, C., Harries, K. A. (2020). Modelling full-culm bamboo as a naturally varying functionally graded material. *Wood Science and Technology, 55(1),* 155–179. DOI 10.1007/s00226-020-01246-6.
39. Tian, L. M., Wei, J. P., Huang, Q. X., Ju, J. W. (2021). Collapse-resistant performance of long-span single-layer spatial grid structures subjected to equivalent sudden joint loads. *Journal of Structural Engineering, 147(1),* 04020309. DOI 10.1061/(ASCE)ST.1943-541X.0002904.
40. Tian, L. M., He, J. X., Zhang, C. B., Bai, R. (2021). Progressive collapse resistance of single-layer latticed domes subjected to non-uniform snow loads. *Journal of Constructional Steel Research, 176(8),* 106433. DOI 10.1016/j.jcsr.2020.106433.
41. Tian, L. M., Kou, Y. F., Lin, H. L., Li, T. J. (2021). Interfacial bond–slip behavior between H-shaped steel and engineered cementitious composites (ECCs). *Engineering Structures, 231(1),* 111731. DOI 10.1016/j.engstruct.2020.111731.